Pre-scission 4He multiplicity in the 19F+197Au reaction

Pre-scission ^{4}He multiplicity in the ^{19}F + ^{197}Au reaction

H. Ikezoe, N. Shikazono, Y. Nagame, Y. Sugiyama, Y. Tomita,
K. Ideno, and A. Iwamoto
Department of Physics, Japan Atomic Energy Research Institute, Tokai-mura, Ibaraki-ken, Japan

T. Ohtsuki
Department of Chemistry, Faculty of Science, Tokyo Metropolitan University, Setagaya-ku, Tokyo, Japan
(Received 22 January 1990)

Pre- and post-scission ^{4}He particle multiplicities for the ^{19}F + ^{197}Au reaction in the excitation energy range of 43 to 90 MeV have been measured in coincidence with fission fragments. The coincident ^{4}He particles measured at backward angles are accounted for by evaporation from a compound nucleus and fission fragments. The most probable center-of-mass energy of the ^{4}He particles measured at backward angles is shifted towards lower energies by ≈ 2 MeV compared to a statistical model calculation performed by assuming ^{4}He emission from a spherical compound nucleus. The observed pre-scission ^{4}He multiplicity as a function of excitation energy is compared to a set of statistical-model calculations which also included the delayed onset of fission. The comparison shows that the observed energy dependence of the pre-scission ^{4}He multiplicity is reproduced by the calculation without taking into account the delayed onset of fission if the reduced emission barrier for ^{4}He is assumed in the calculation. The emission mechanism of the pre-scission ^{4}He is discussed.

I. INTRODUCTION

The fission process can be viewed as a dynamical motion of the nucleus from a nearly spherical shape to a scission shape. The time scale which characterizes this motion has been investigated theoretically[1-6] and experimentally.[7-25] The diffusion model, applied to fission, predicts a transient time defined as the time needed for a fission width to rise from 0% to 90% of its stationary value at the saddle point. This transient time affects particle evaporation before fission. Experimentally much evidence indicates a long transient time or a long transition time during the descent from saddle to scission compared to particle evaporation lifetimes at high excitation energy. For example, at high excitation energies ($U \geq 150$ MeV), a large number of pre-scission charged particles has been observed.[7-19] The observed pre-scission neutron multiplicities[20-25] are about two times larger than the predicted values of statistical-model calculations at excitation energies $U \geq 100$ MeV. These enhancements of the pre-scission particle multiplicities indicate that the lifetime of fission is relatively longer than those for particle evaporation. Consequently, particles can evaporate before the compound-nucleus fissions.

The lifetimes for particle evaporation from a compound nucleus with a given excitation energy and a given angular momentum can be calculated in the framework of the statistical model. Then, information relating to the fission time scale can be obtained by measuring the number of particles evaporated before the compound-nucleus fissions. Although both charged particles and neutrons emitted before fission give information on the time scale of fission, it should be noted that the emission mechanism is not the same for both. Neutron emission is not very

sensitive to the deformation of the compound nucleus, so they can be emitted at any stage of the fission process. On the other hand, the emission probability for charged particles depend strongly on the Coulomb barrier height between the particle and the daughter nucleus and hence on the deformation of the daughter nucleus. In this sense, a pre-scission charged particle can be a promising probe for sensing the deformation of a fissioning nucleus.

In the present work, we measured the pre- and post-scission ^{4}He multiplicities in the ^{19}F + ^{197}Au reaction as a function of the excitation energy of the compound nucleus. On the bases of the measured energy spectra and pre-scission ^{4}He multiplicity, the emission mechanism of ^{4}He is discussed.

II. EXPERIMENTAL PROCEDURE

A self-supported ^{197}Au target of a thickness of 1.2 mg/cm^2 was bombarded with a ^{19}F beam from the JAERI tandem accelerator. The experiments were performed with bombarding energies (E_{lab}) from 92 to 161 MeV. The lowest bombarding energy is just above the Coulomb barrier for the ^{19}F + ^{197}Au system. Fission fragments were measured by an ionization chamber detector (IC) in the inclusive measurements and by two solid-state detectors (SSD, 60 μm, 400 mm^2) with large solid angles (36 and 55 msr) in the coincidence measurements. The IC is composed of an anode to measure the energy loss ΔE of reaction products in the 10 Torr of isobutane gas in the chamber, and a solid-state detector (300 μm, 300 mm^2) to measure their residual energy E. A polyester foil of a thickness 70 μg/cm^2 was used as a window. The two fission detectors were set up at $\theta_f = 105°$ and 125° (with respect to the beam), respectively. The angular distribu-

tion of the fission fragments were measured with the IC at backward angles $\theta_{\mathrm{lab}} \geq 90°$.

A two-dimensional display of E vs ΔE measured by the IC showed that almost all the reaction products detected at backward angles were fission fragments and light ions at bombarding energies higher than 100 MeV. The energy spectra of the reaction products measured by the SSD at $\theta_f = 125°$ in coincidence with light charged particles (proton and ⁴He) are shown in Fig. 1. As shown on the left side of the figure, the fission fragments and the light ions (the low energy peak) are well separated and there are no contributions of projectile-like products in the energy spectrum.

At the lower bombarding energies of 92 and 99 MeV, the backward SSD at $\theta_f = 125°$ was used to detect the fission fragments. In this measurement, detected fission fragments and projectile-like products partly overlapped each other in energy, because of the large grazing angles of 112° for 99 MeV and $\approx 180°$ for 92 MeV. In order to detect the fission fragments separately from the projectile-like products, a thin polyester foil (140 μg/cm²) was put in front of the SSD. As shown on the right side of Fig. 1, the fission fragments are well separated from the projectile-like products (the high energy peak in Fig. 1) due to the difference of their energy losses in the thin foil.

Light particles (⁴He and protons) were measured by three sets of solid-state detector telescopes (30 and 2000 μm) positioned at inplane ($\phi = 90°$) and out-of-plane angles ($\phi = 30°$ and 60°). Here, inplane is the plane defined by the direction of the beam and a detected fission fragment. The out-of-plane angle ϕ is the angle between the normal of the inplane and the direction of the detector telescope. These telescopes were set at inplane negative

angles ($\theta_{\mathrm{lab}} = -135°$ and $-145°$) in the coincidence measurements. Here, the negative angle is the angle on the side opposite to the SSD with respect to the beam. Energy calibrations for each solid-state detector were obtained with an ²⁴¹Am source and a precision pulser.

III. EXPERIMENTAL RESULTS

A. Inclusive ⁴He spectrum

The inclusive energy spectra and the angular distribution of ⁴He were measured at a bombarding energy of 138 MeV. A velocity contour map of the invariant cross section for the inclusive ⁴He emission is shown in Fig. 2, where the measured velocity was decomposed into the parallel $V_{\parallel}$ and the perpendicular $V_{\perp}$ components with respect to the beam direction. The velocity corresponding to a specified value of the relative yield in the invariant velocity spectra was plotted as a length from the origin of the contour map. The circular arcs centered on the velocity V_{cm} of the compound nucleus reproduce the backward data ($\theta_{\mathrm{lab}} > 90°$) very well. This suggests that the ⁴He particles measured at backward angles originate mainly from the evaporation of the compound nucleus.

The inclusive energy spectrum of ⁴He is shown in Fig. 3 as the solid line. The ⁴He energy measured at $\theta_{\mathrm{lab}} = -150°$ was transformed to the center of mass system assuming evaporation from the compound nucleus. The result of the statistical-model calculation is also shown by a dashed line, where the statistical-model code PACE (Ref. 26) was used. The optical-model potential parameters of Ref. 27 were used for the ⁴He evaporation. A level-density parameter $a = A/8$ MeV⁻¹, where A is the mass number, was assumed. The absolute yield of the calculated spectrum was normalized to the data. It is seen that the observed most probable energy is shifted to-
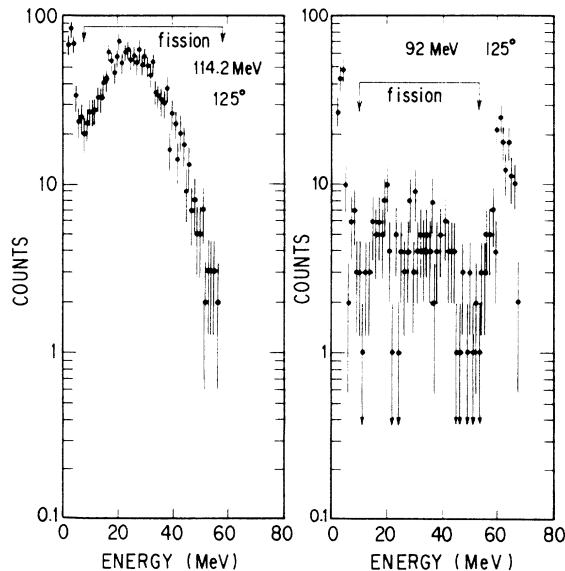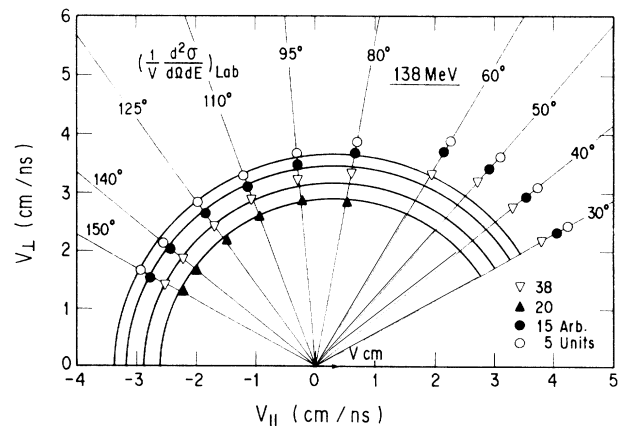

FIG. 1. Energy spectra of fission fragments measured by the SSD in the coincidence measurements at the bombarding energies 114.2 and 92 MeV.

FIG. 2. Velocity contour map of an invariant cross section for inclusive ⁴He emission at the bombarding energy of 138 MeV. The measured velocity was decomposed of the parallel $V_{\parallel}$ and the perpendicular $V_{\perp}$ components with respect to the beam direction. V_{cm} is the c.m. velocity. The arcs are centered on V_{cm}. The straight lines from the origin represent the detection angles.

ward lower energies compared with the calculated result.

In order to extract an effective emission barrier for ^{4}He, the transmission coefficients as a function of the kinetic energy of ^{4}He were artificially shifted toward lower energies by 2 MeV. The calculation with this modification is shown in Fig. 3 as the dashed-dotted line. The calculated shape reproduces the data very well. This suggests that the effective emission barrier for ^{4}He decreases by an amount of 2 MeV in the present system. A similar phenomenon has been observed for the evaporation spectrum of ^{4}He in many other reaction systems.[28-30] According to Ref. 28, the energy difference between the observed emission barrier and the absorption barrier systematically increases as the reaction system becomes heavier. The present result (2-MeV shift) agrees with the systematic trend of Ref. 28. The present result was also confirmed by analyzing the energy spectra of ^{4}He measured in coincidence with fission fragments as discussed in Sec. III C. We also observed a shift of about 1 MeV of the most probable energy toward lower energies in the inclusive proton energy spectrum compared with the calculation, where the optical-model potential parameters of Ref. 31 were used for the proton evaporation.
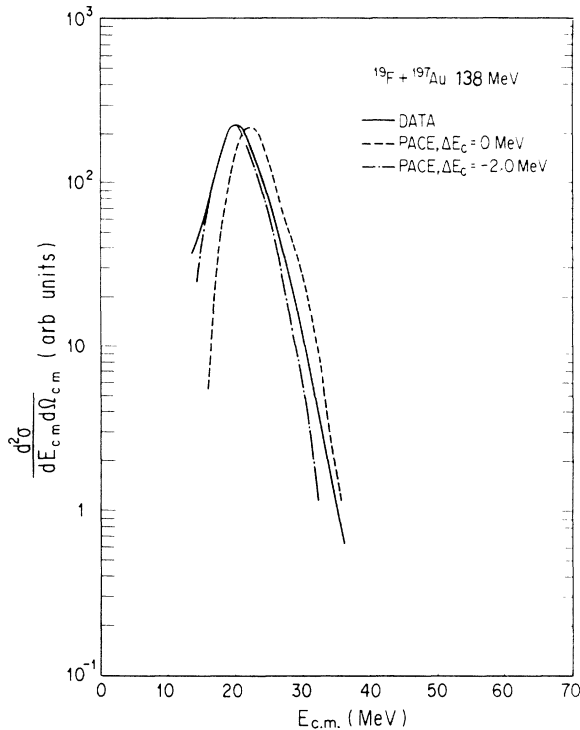

FIG. 4. Fission cross section as a function of the bombarding energy. The prediction of the Bass model is shown as the solid line.

B. Cross section of fission

The angular distributions of the inclusive fission fragments were measured with the IC. The measured angular distributions as a function of the bombarding energies have been reported in Ref. 32. The cross section of fission was obtained by integrating the angular distribution transferred to the center-of-mass system assuming the total kinetic energy (TKE) of the fission fragments predicted by the Viola's systematics.[33] Absolute values of the cross sections were obtained by normalizing the fission yields to the elastic scattering cross section of ^{19}F. The cross sections of fission σ_{fiss} are listed in Table I and are plotted in Fig. 4 as a function of the bombarding energy.

The measured fission cross sections were compared with a statistical-model calculation in which the fusion cross section was predicted by the Bass model.[34] The ratio a_f/a_n of the level-density parameters at the saddle point and the ground-state deformations was assumed to

FIG. 3. Inclusive c.m. energy spectrum of ^{4}He (solid line) measured at the bombarding energy of 138 MeV. The dashed line is the result of the statistical-model calculation using the code PACE. The dashed-dotted line is the result calculated by assuming the 2-MeV shifted transmission coefficient toward lower energies.
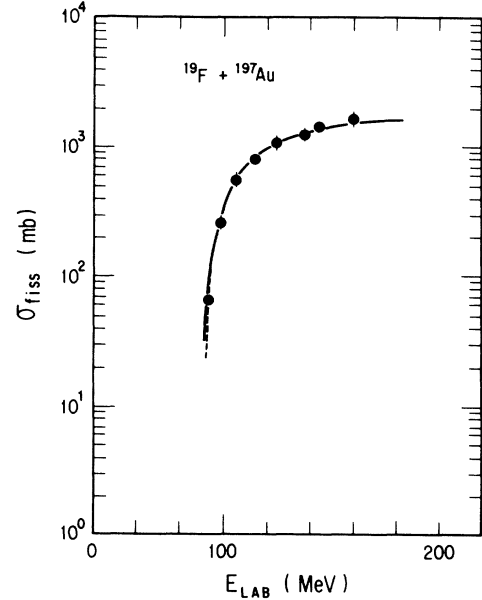
TABLE I. Fission cross sections as a function of the bombarding energy.

E_{lab}(MeV)	U(MeV)	σ_{fiss}(mb)
92	43.4	68±7
99	50.0	273±30
106.1	56.2	579±58
114.2	63.6	841±85
125	73.5	1110±120
138	85.4	1270±100
145	91.7	1470±140
161	106.3	1690±140

be unity and the fission barrier height B_f was calculated by the rotating finite range model (RFRM).[35] The solid line in Fig. 4 represents the fusion cross section predicted by the Bass model. The calculated fission cross section (dashed line) was about 90% of the fusion cross section at the lowest bombarding energy and became nearly equal to the fusion cross section at the higher bombarding energies. The overall agreement between the measured fission cross sections and the calculated result is good.

C. Coincidence spectra

In general, there are three different sources for particle emission, evaporations from fission fragments (FE), compound-nucleus emission (CE), and pre-equilibrium emission (PE). Since ^{4}He particles were detected at backward angles ($\theta_{lab} = -135°$ and $-145°$) in the coincidence measurements, contributions from PE are negligible. The coincidence data were analyzed by taking into account two emission sources, FE and CE.

In the present work, we concentrated our attention on the coincidence measurements between the fission fragments and the ^{4}He particles because it was experimentally easy to identify the emission sources of these ^{4}He particles. This identification was rather difficult for the protons because the difference of the Coulomb barrier heights are not very large for the two emitters (FE and CE).

The energy spectra of ^{4}He measured in coincidence with the fission fragments are shown in Figs. 5 and 6. The ordinate is defined as

$$d^2M/dE_\alpha d\Omega_\alpha = (d^3\sigma/dE_\alpha d\Omega_\alpha d\Omega_{fiss})/(d\sigma/d\Omega_{fiss}) ,$$

where $d\sigma/d\Omega_{fiss}$ is the inclusive cross section of the fission fragments at the angle where the fission fragments were measured in the coincidence measurements. The dashed and the dashed-dotted lines represent the calculated energy spectra corresponding to the emission sources of CE and FE, respectively.

The ^{4}He energy spectra from FE were calculated by the code PACE assuming the following input parameters. The excitation energy E_f of the fission fragments were estimated using the Q value for symmetric mass division and the TKE predicted by the Viola's systematics:

$$E_f = (U - Q - \text{TKE})/2 , \tag{1}$$

where U is the excitation energy of the compound nucleus. An average angular momentum for both fission fragments was estimated to be $2/7\bar{l}$ by assuming the sticking limit for two touching fragments. Here, $\bar{l}$ is the average angular momentum for the fissioning nucleus; $\bar{l}$ was estimated by the PACE calculation assuming the fusion cross section predicted by the Bass model. Transmission coefficients of ^{4}He for FE were calculated using the optical-model potential[27] without any modification, because the energy difference between the effective emission barrier and the corresponding absorption barrier is expected to be small[28] for light nuclei like fission fragments.

The ^{4}He energy spectrum for CE at each bombarding energy was calculated by assuming an effective emission barrier for ^{4}He. These transmission coefficients were shifted toward lower energies by 2 MeV. The calculated spectra (CE and FE) shown in Figs. 5 and 6 were obtained by transforming the calculated center-of-mass kinetic energy spectra to the laboratory frame. The orien-
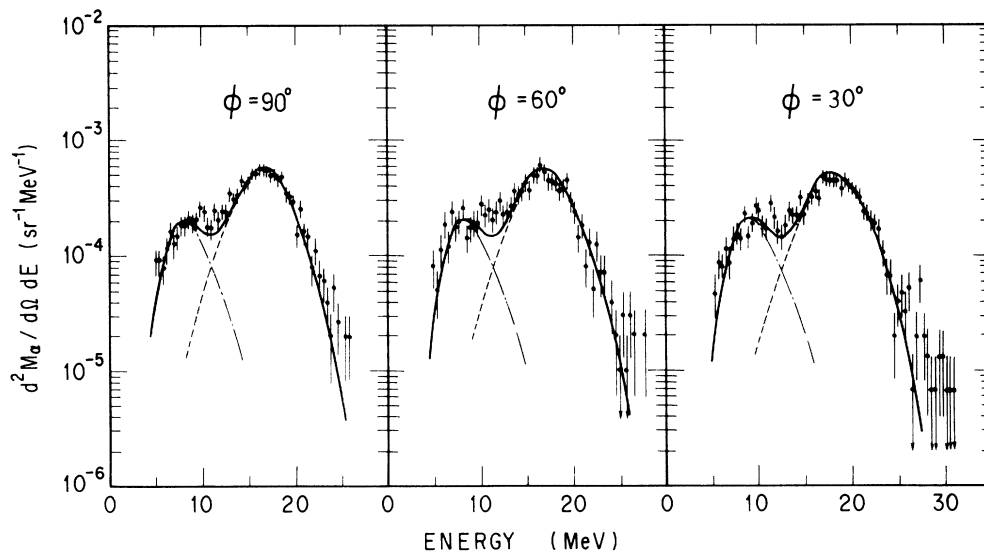

FIG. 5. Energy spectra of ^{4}He in coincidence with the fission fragments at the bombarding energy of 137 MeV. The fission fragment and ^{4}He were detected at $\theta_f = 105°$ and $\theta_{lab} = -145°$, respectively. The dashed and the dashed-dotted lines represent the calculated spectra corresponding to the emission sources of CE and FE, respectively. The solid lines show the sum of the two components. The out-of-plane angle ϕ is defined as an angle between the normal to the reaction plane and the emission direction of ^{4}He.
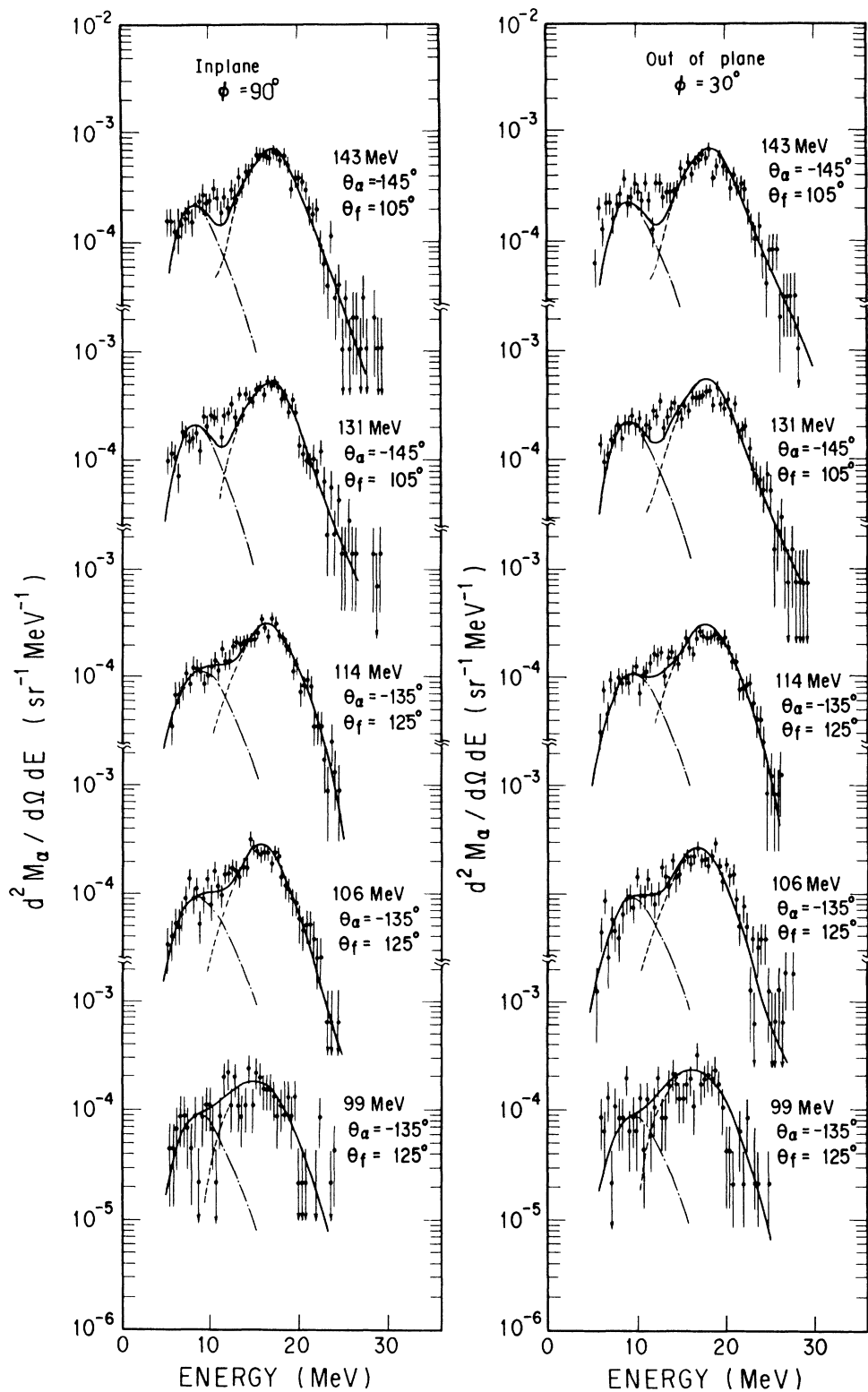
FIG. 6. Same as Fig. 5 for the various bombarding energies indicated, where θ_f and θ_a are the inplane angles of the fission detector SSD and the ^{4}He counter telescope with respect to the beam.

tation of the angular momentum of the compound nucleus which could be oriented perpendicular to the reaction plane in the coincidence experiment (by detecting the fission fragments) was neglected in the present calculation.

The calculated energy spectra for FE and CE were simultaneously fitted to the inplane and the out-of-plane data by adjusting normalization factors, where the angular distribution of the ^{4}He emitted from FE was assumed to be isotropic in the rest frame of the fission fragments. This assumption can be justified because of the small angular momentum of the fission fragments (the average angular momentum of each fragment is estimated to be ~$7\hbar$ at $E_{lab}=138$ MeV by assuming the sticking limit). The shape of the ^{4}He energy spectra for FE depends strongly on the relative emission angle between the fission fragment and ^{4}He. In Figs. 5 and 6, the ^{4}He evaporations from the detected and the undetected fragments overlap each other in energy.

The observed coincidence energy spectra of ^{4}He were well reproduced by the calculated two components (FE and CE). The mean center-of-mass (c.m.) kinetic energies $\langle\epsilon\rangle$ for CE measured inplane are plotted as a function of excitation energy in Fig. 7. The observed $\langle\epsilon\rangle$ of the compound nucleus is well reproduced by the calculation (solid line), where the transmission coefficient for ^{4}He was shifted toward lower energies by 2 MeV. The dashed line shows the calculated result without shifting the transmission coefficient toward lower energies. From this result we confirmed that the effective emission barrier for ^{4}He was smaller by 2 MeV than the corresponding absorption barrier.

FIG. 8. Post-scission ^{4}He multiplicity as a function of the compound-nucleus excitation energy U. The solid line is the result of the PACE calculation using the fragment excitation energy calculated by Eq. (1).
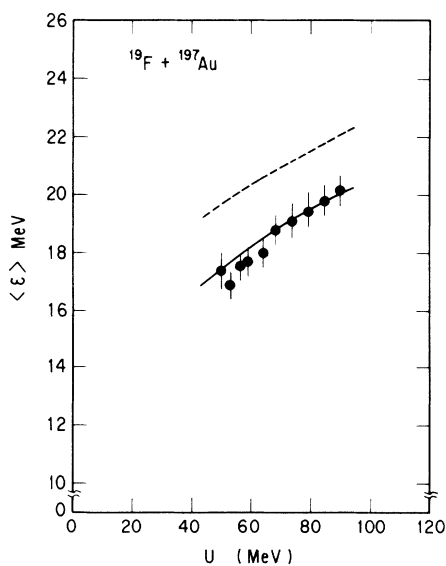

FIG. 7. The mean c.m. kinetic energy of CE as a function of the compound-nucleus excitation energy U. The solid line indicates the calculated result by assuming the 2-MeV reduced barrier for ^{4}He. The dashed line indicates the calculated result by assuming the normal emission barrier which is the same as the respective absorption barrier.
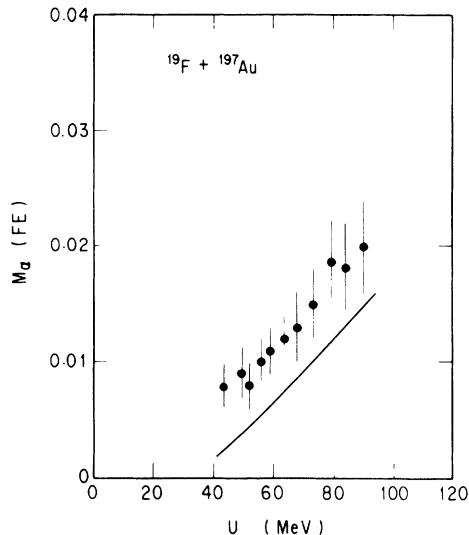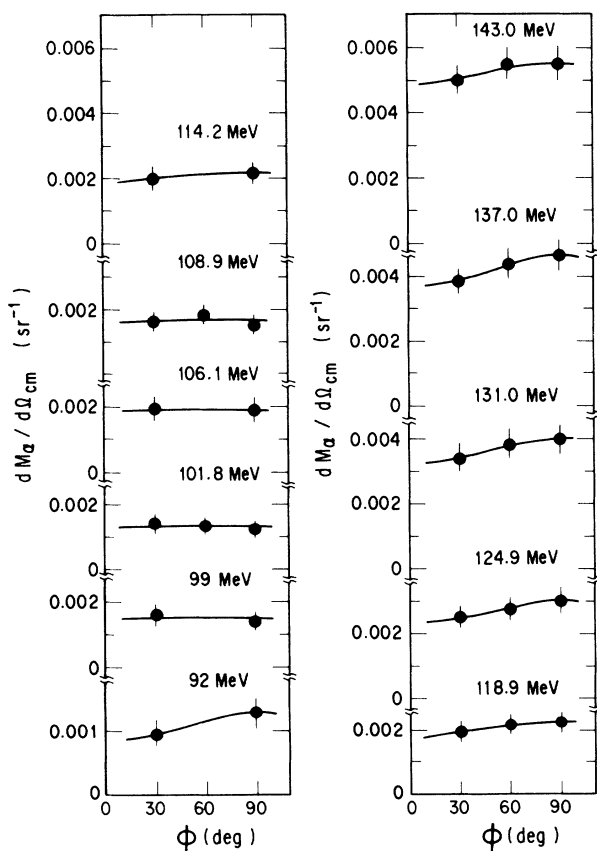

FIG. 9. Differential pre-scission multiplicities of ^{4}He as a function of the out-of-plane angle ϕ for various bombarding energies.

TABLE II. Pre- and post-scission multiplicities of ^{4}He as a function of the bombarding energy.

E_{lab}(MeV)	U(MeV)	$M\alpha$(CE)	$M\alpha$(FE)
92	43.4	0.014±0.003	0.008±0.002
99	50.0	0.019±0.004	0.009±0.002
101.8	52.3	0.017±0.003	0.008±0.002
106.1	56.2	0.025±0.005	0.010±0.002
108.9	58.8	0.021±0.004	0.011±0.002
114.2	63.6	0.026±0.005	0.012±0.002
118.9	67.9	0.026±0.005	0.013±0.003
124.9	73.4	0.035±0.006	0.015±0.003
131.0	78.9	0.047±0.007	0.019±0.003
137.0	84.4	0.054±0.010	0.018±0.004
143.0	89.9	0.066±0.010	0.020±0.004

D. Post-scission multiplicity of ^{4}He

The FE components were integrated to obtain the post-scission ^{4}He multiplicities by assuming an isotropic angular distribution in the fragment rest frame. These multiplicities are listed in Table II as M_α(FE) and plotted in Fig. 8.

E. Pre-scission multiplicity of ^{4}He

An intermediate energy component between CE and FE was observed at the highest bombarding energies ($E_{lab} > 114$ MeV) as can be seen in Figs. 5 and 6. In the present experimental setup, the ^{4}He detectors (both the

FIG. 10. Pre-scission ^{4}He multiplicity as a function of excitation energy. The PACE calculation (solid line) was performed by assuming $a_f/a_n = 1.00$ and the fission barrier $B_f = B_{RFRM}$, where B_{RFRM} is the calculated value by the rotating finite range model. The dashed line indicates the calculated result by taking into account the effect of the delayed onset of fission, where the delay time τ_d is assumed to be 80×10^{-20} sec. In this calculation the emission barrier of ^{4}He was assumed to be the same as the respective absorption barrier.

inplane and out-of-plane detectors) were positioned at angles nearly perpendicular (within ±15°) to the emission direction of the fission fragments. The intermediate component has a mean center-of-mass energy of 13–14 MeV which is estimated by assuming that this component originates from compound-nucleus emission. This mean energy is slightly less than the energy (about 16 MeV) of a scission ^{4}He.[36,37] Although the angular distribution of this component with respect to the emission direction of the fission fragments was not measured, its relative yield was small compared with the two components (CE and FE) as shown in Figs. 5 and 6. In order to obtain the CE component, this intermediate component and the FE component were subtracted from the coincidence spectra.

The differential pre-scission multiplicities $dM_\alpha/d\Omega_{cm}$ were obtained by integrating the CE component in energy and correcting the solid angle ratio between the laboratory frame to the center-of-mass frame. The $dM_\alpha/d\Omega_{cm}$ are shown in Fig. 9 as a function of the out-of-plane angle ϕ. The out-of-plane angular distribution was fitted by a function $W_0\exp(\beta_2\sin^2\phi)$,[38] where W_0 and β_2 were the fitting parameters. The fitted curves are shown as the solid lines in Fig. 9. The obtained β_2 values for the data measured at $E_{lab} \geq 114.2$ MeV were 0.1–0.24. The out-of-plane angular distributions at the bombarding energies from 99 to 108.9 MeV were nearly independent of ϕ.

The pre-scission multiplicities of ^{4}He were obtained by integrating the out-of-plane angular distribution. These are listed in Table II as M_α(CE) and are plotted in Fig. 10 as a function of the excitation energy of the compound nucleus.

IV. DISCUSSION

A. Mean kinetic energy of the pre-scission ^{4}He

As mentioned in Secs. III A and III C, the effective emission barrier of ^{4}He was smaller by an amount of 2 MeV than the corresponding absorption barrier. As to a mechanism which causes this reduced emission barrier, many authors[14,28–30,39–41,42] have claimed a deformation of the compound nucleus, because the Coulomb barrier between ^{4}He and a deformed nucleus is smaller at the tip of a long axis than the one between ^{4}He and a spherical nucleus. Energy spectra and angular distributions of ^{4}He evaporated from CE have been accounted for by assum-

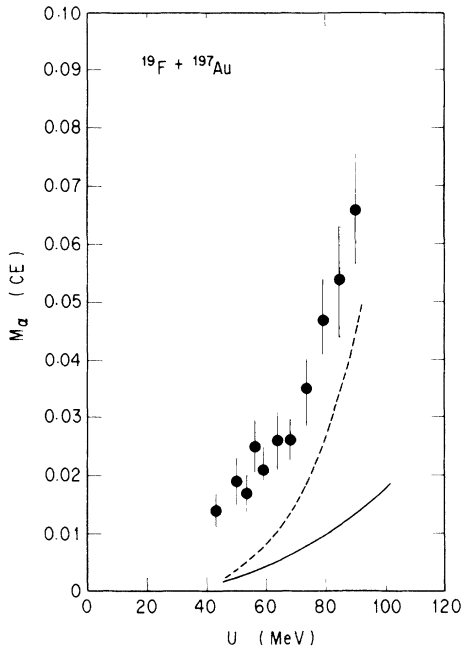ing some deformations of compound nuclei, while more elongated shapes of compound nuclei than those for ^{4}He have been required to reproduce peak energy shifts of proton energy spectra.[29,30,40] Up to now there is no satisfactory theory to explain consistently the causes of both the reduced emission barriers of proton and ^{4}He.[29]

Since in the coincidence experiments the angular momentum could be oriented perpendicular to the reaction plane, the energy spectra and the anisotropy of the out-of-plane angular distribution may give us some information about the compound-nucleus deformation. The observed mean c.m. kinetic energies of ^{4}He were nearly independent of ϕ and the energy spectra were reproduced by the calculation where the angular momentum orientation was neglected. The mean c.m. kinetic energy is theoretically given by the sum of the emission barrier, the nuclear temperature, and the centrifugal barrier due to the exit channel orbital angular momentum.[39] If the compound nucleus is deformed with a prolate shape and the nuclear symmetry axis is ideally oriented at $\phi = 90°$ (inplane), the mean c.m. kinetic energy should be minimum at $\phi = 90°$ and maximum at $\phi = 0$.[39] However the ideal orientation of the angular momentum is not achieved at a finite temperature. In this case the dependence of the mean kinetic energy on ϕ might be smeared out by a broad K distribution, where K is the projection of the compound nucleus angular momentum J on the nuclear symmetric axis. As reported in Ref. 32, the angular distribution of the fission fragments in the present reaction system is well reproduced by the calculation using the K distribution calculated by the RFRM. The predicted K_0^2 value, which is a parameter to determine the K distribution,[45] is $160\hbar^2$ at the nuclear temperature $T = 1.5$ MeV ($T = \sqrt{U/a}$). This corresponds to the half width of the half maximum (HWHM) of $15\hbar$ of the K distribution. According to the PACE calculation, the average value $\langle J \rangle_\alpha$ of the entrance channel angular momenta which contribute to the pre-scission ^{4}He emission is nearly constant ($\langle J \rangle_\alpha^{cal} \simeq 33\hbar$) for the reactions with $E_{lab} \geq 114.2$ MeV, although the average value $\langle J \rangle_f$ of the entrance channel angular momenta contributing to the fission process increases with the bombarding energy. Since the HWHM of $15\hbar$ is almost a half of $\langle J \rangle_\alpha$, it turns out that the angular momentum orientation of the compound nucleus is considerably smeared out. This broad K distribution may result in the small anisotropy parameter β_2 and shade off the dependence of $\langle \epsilon \rangle$ on ϕ.

As shown in Fig. 7, the observed mean c.m. kinetic energy increases with U in the similar manner as predicted by the statistical model. Since the decay width of ^{4}He depends strongly on the excitation energy, the first chance emission is more favorable than the second or third chance emission for ^{4}He. The PACE calculation shows that in the ^{4}He emission cascades the first and second chance emissions are predominant (more than 80%). If third or the fourth chance emission is predominant (that is, if two or three neutron emissions precede ^{4}He emission), the mean c.m. kinetic energy would be smaller than the observed values. This is because one neutron emission preceding ^{4}He emission can remove about 10 MeV (binding energy $+2T$) of excitation energy. The observed

trend of the mean c.m. kinetic energy as a function of U supports the result of the PACE calculation.

B. Post-scission ^{4}He

The statistical-model calculation for ^{4}He emission from the excited fission fragments was performed as mentioned in Sec. III C. In this calculation we neglected the neutron emission prior to scission and then the fragment excitation energy was calculated by Eq. (1). This assumption is not correct because two to four pre-scission neutrons are emitted[23,25] on average in the present excitation energy region. In addition, a part of the excitation energy is removed by the pre-scission neutrons. It was pointed out[43] that the fragment temperature 1.5 MeV is independent because the number of pre-scission neutrons increases with U. On the contrary, the observed post-scission ^{4}He increases as U increases (Fig. 8) in the same manner predicted by the calculation (solid line). The temperature of the fission fragments calculated using Eq. (1) ranges from 1.4–1.9 MeV in the present bombarding energy region. This contradiction is qualitatively explained as follows. According to the PACE calculation, the ^{4}He particle decay width increases more rapidly than the neutron decay width as the excitation energy increases. This means that the ratio of the ^{4}He emission rate to that for neutron increases with the excitation energy. In addition to this fact, the excitation energy of the fission fragments distributes around a mean value due to the broad mass[32] and the total kinetic energy distributions of the fission fragments and also the statistical fluctuation of the pre-scission neutron multiplicity. From these considerations it is presumed that ^{4}He is emitted preferably from a higher fragment excitation energy region than the one for neutrons. Even if the mean excitation energy of the fragments does not increase with U as indicated by the post-scission neutron multiplicity data,[43] the post-scission ^{4}He emission can increase because the distribution of the fragment excitation energy becomes broader as the bombarding energy increases.

C. Pre-scission ^{4}He

In Fig. 10 the observed pre-scission multiplicity for ^{4}He is compared with a standard statistical-model calculation without any modification of the transmission coefficient for ^{4}He. The liquid drop masses of Ref. 44 were used to calculate the excitation energies of the compound and daughter nuclei and the fission barrier heights were calculated by the RFRM. The neutron, proton, ^{4}He, and gamma-ray emission was taken into account in addition to fission. The entrance channel angular momentum distribution for fusion was determined by the sharp cutoff approximation, where the diffuseness parameter δ_l was fixed to be $0.5\hbar$.

The calculated result (solid line) underestimates considerably the pre-scission multiplicity even at the low excitation energies $U \leq 60$ MeV, where the effect of the delayed onset of fission on particle emission is expected to be small.[23–25] It is expected that the emission probability for ^{4}He increases with decreasing emission barriers. In order to improve the calculation, the 2-MeV reduced

emission barrier of ^{4}He was taken into account. In the present analysis, we did not calculate the transmission coefficient of ^{4}He for a deformed nucleus, but the transmission coefficients which were calculated using the optical-model parameters for proton[31] and for ^{4}He[27] were shifted toward lower energies by 2 MeV and 1 MeV for ^{4}He and proton, respectively, so that the inclusive and the coincidence energy spectra were reproduced. The adopted 1-MeV reduced barrier for the proton was simply based on the inclusive measurement of the proton energy spectra at backward angles. The calculated result of the pre-scission ^{4}He multiplicity was insensitive to the adopted 1-MeV reduced barrier for protons.

The results of the calculation are shown in Fig. 11, where the value of the ratio a_f/a_n was varied to see the dependence of the calculated M_α(CE) on the excitation energy. The calculated results are sensitive to the value of this ratio especially in the high excitation energy region. As shown in Figs. 10 and 11 the effect of the reduced emission barrier on M_α(CE) is large. This means that the calculated M_α(CE) depends strongly on the precision of the effective emission barrier of ^{4}He. The required reduction of 2 MeV of the effective emission barrier is much larger than the experimental error (≤ 0.5 MeV).

The sharp cutoff approximation for the entrance channel angular momentum distribution may not be adequate. It is reported that the angular momentum distribution for fusion extends to high l values in the sub-barrier fusion.[45]
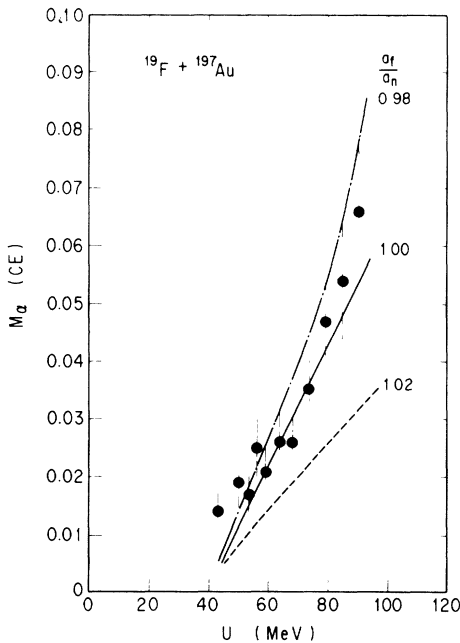

FIG. 11. Same as Fig. 10. The PACE calculation with various values of a_f/a_n are shown by taking into account the measured effective emission barrier of ^{4}He. In this calculation the effect of the delayed onset of fission is not included.

The effect of the broad distribution of the entrance channel angular momentum on the pre-scission ^{4}He multiplicity was examined by assuming the various values of $\delta_l;\delta_l = 5$ and $10\hbar$. It was found that the calculated M_α(CE) was rather insensitive to δ_l even at the low bombarding energies of 99 and 92 MeV. This is due to the fact that the fission probability increases with l while that for ^{4}He evaporation decreases at high l values. Therefore, the ^{4}He evaporation followed by fission gradually decreases at high l values.

D. Emission mechanism of pre-scission ^{4}He

As shown in Fig. 11, the excitation energy dependence including the absolute value of the observed pre-scission ^{4}He multiplicity was reproduced by the present calculation assuming $a_f/a_n = 0.98 - 1.00$ and $B_f = B_{RFRM}$ and by taking into account the 2-MeV reduced emission barrier.

As mentioned previously, it is reported that the observed pre-scission neutron multiplicities[20-25] are about two times larger than the prediction of the statistical model. These excess neutron emissions before fission have been ascribed to the emission during the delayed onset of fission (a nonzero transient time) and/or a long transition time during the descent from saddle to scission. In this consideration, it is assumed that the neutron decay width is independent of the time evolution of the excited compound nucleus toward fission, while the fission width grows as a function of time. If the decay width of ^{4}He is also independent of the time evolution, the delay time of the fission onset should result in an enhancement of the pre-scission ^{4}He emission in a manner similar to that for pre-scission neutrons. This is illustrated as the dashed line in Fig. 10, where a long time delay $\tau_d = 80 \times 10^{-20}$ sec of the fission onset was assumed and the emission barrier of ^{4}He was assumed to be the same as the respective absorption barrier. The calculation procedure incorporating the delayed onset of fission is shown in the Appendix. The calculated result (dashed line) increases considerably at $U > 60$ MeV but still underestimates the pre-scission ^{4}He multiplicity even if we assume a large delay time which exceeds the upper limit reported in Ref. 25. When we take into account the 2-MeV reduced barrier for ^{4}He together with the reported delay time of the fission onset (typically 10^{-19} sec),[23,25] the calculated pre-scission ^{4}He multiplicity becomes larger than two times that of the present data. The present analysis shows that it is not necessary to assume the delayed onset of fission in the calculation in order to reproduce the observed pre-scission ^{4}He multiplicity. This contradiction may be ascribed to the difference of the emission mechanisms between neutron and ^{4}He.

In order to investigate the emission mechanism, the ratio of the pre-scission multiplicities of the neutron to ^{4}He was plotted as a function of U in Fig. 12. For the pre-scission neutron multiplicity M_n, the data for the ^{16}O + ^{197}Au reaction[25] were used, because the compound nuclei of this reaction and the present system have similar mass (213 and 216) and fissility (0.74). The pre-scission neutron data were fitted by a linear function of U
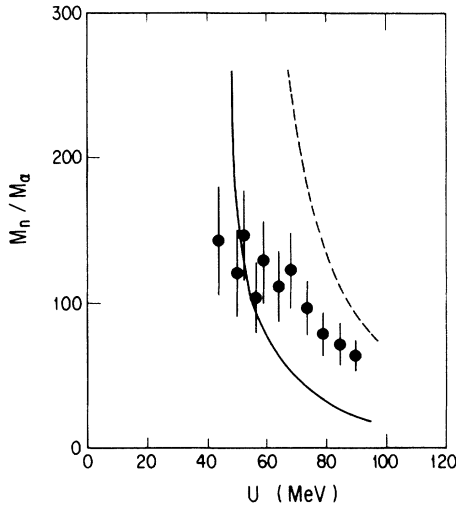
FIG. 12. Ratio of the pre-scission multiplicities of neutron to ^{4}He as a function of the excitation energy of the compound nucleus. The data of the pre-scission neutron multiplicity were adopted from Ref. 25.

from 45 to 120 MeV and the values corresponding to the present excitation energies were extracted with errors of 0.3–0.4 neutrons. The errors shown in Fig. 12 are mainly ascribed to the experimental uncertainty in the pre-scission ^{4}He multiplicity measurement. The ratio is roughly equal to the ratio of the decay widths of the pre-scission neutron to the pre-scission ^{4}He. The solid and the dashed lines shown in Fig. 12 are the calculated results assuming the 2-MeV reduced emission barrier and the corresponding absorption barrier for ^{4}He, respectively. The ratio is not sensitive to the level-density parameter and the a_f/a_n ratio.

The calculated result (solid line) agrees with the observed ratio M_n/M_α at low excitation energies ($U \leq 60$ MeV). As U increases, the ratio deviates from the solid line and approaches the dashed one. This phenomenon indicates that one of the decay widths (neutron or ^{4}He) differs from the statistical-model prediction. The neutron decay width is reasonably assumed to be insensitive to deformations of the fissioning nucleus and well simulated by the statistical-model calculation, while the decay width of ^{4}He depends on the deformations and may increase with the deformations from a value corresponding to a spherical shape to a stationary value corresponding to the saddle deformation. The decay width calculated by assuming the 2-MeV reduced emission barrier may correspond to the stationary value. When the fission lifetime is long enough compared with a time needed for the decay width of ^{4}He to increase to the stationary value, an effective decay width of ^{4}He averaged in time during the fission lifetime is close to the stationary value. In this case the ratio M_n/M_α is close to the value shown by the solid line. As U increases, the fission lifetime becomes shorter. When the fission lifetime becomes comparable to the time needed for the decay width of ^{4}He to grow up to the stationary value, the averaged decay width of ^{4}He during the fission lifetime becomes smaller than the stationary value.

This can cause the observed deviation of the M_n/M_α from the solid line, and brings the ratio closer to the dashed line.

If the decay width of ^{4}He grows on a similar time scale to that for the fission width, the delayed onset of fission has little effect on the pre-scission ^{4}He emission. This is because the ratio of the decay width of ^{4}He to that for fission becomes essentially independent of time. In this case it is not necessary to include the delayed onset of fission in the calculation of the pre-scission ^{4}He multiplicity. In fact if the delayed onset of fission is included in the calculation, the time dependence of the decay width of ^{4}He has to be taken into account together with the delayed onset of fission.

During the descent from saddle to scission, ^{4}He may be emitted. In order to estimate this emission probability for ^{4}He, it is necessary to treat the dynamical motion of the fission process. According to the calculation of Ref. 46, the ^{4}He emitted during the descent from saddle to scission tends to concentrate in a direction perpendicular to the fission direction. This tendency becomes remarkable for ^{4}He particles emitted near the scission shape, due to Coulomb focusing caused by both parts of the "snapping" compound nucleus.[47] As mentioned at Sec. III E, the observed intermediate energy component was relatively small compared with the components of FE and CE. In fact, the yield of these pre-scission ^{4}He particles is 0.003–0.006 per fission event[15,37,48−50] in the excitation energy region of $U \leq 100$ MeV. These values are one order of magnitude smaller than the observed pre-scission CE ^{4}He multiplicities. The observed pre-scission ^{4}He then has to be attributed to the compound-nucleus emission from a stage of the fission process before the descent from saddle to scission.

The present PACE calculation was applied to the pre-scission ^{4}He multiplicity data, $M_\alpha(\text{CE})=0.010\pm0.003$ and 0.025 ± 0.006, measured in the ^{16}O+^{232}Th and ^{12}C+^{197}Au reactions,[37] respectively. In this calculation the 2-MeV reduced emission barrier for ^{4}He was assumed as in the present system. The ratio a_f/a_n was assumed to be unity. The calculated results were 0.009 and 0.025 for the ^{16}O+^{232}Th and ^{12}C+^{197}Au reactions, respectively and reproduced the data without including the delayed onset of fission. This is consistent with the present experimental results.

V. SUMMARY AND CONCLUSIONS

We have measured pre- and post-scission ^{4}He emission in coincidence with fission fragments in the ^{19}F+^{197}Au reaction. The ^{4}He measured at backward angles in coincidence with these fragments are accounted for by evaporations from the compound nucleus and fission fragments. The mean cm kinetic energy for CE observed in the coincidence measurement is smaller (by 2 MeV) than the value predicted by assuming evaporation from a spherical compound nucleus. This means that the effective emission barrier of ^{4}He is reduced by 2 MeV compared to the corresponding absorption barrier. The obtained pre-scission multiplicity of ^{4}He, as a function of the excitation energy, is reproduced by the statistical-

model calculations which take into account this reduced emission barrier. The effect of the delayed onset of fission has not been observed on the pre-scission ^{4}He multiplicity. The observed ratio of M_n/M_α suggests that there is a difference between the emission mechanisms for pre-scission neutrons and ^{4}He. These results support the conjecture that the decay width of ^{4}He grows with the deformation of the fissioning nucleus on a similar time scale to that for the growth of the fission width.

ACKNOWLEDGMENTS

APPENDIX

We have examined the effect of the delayed onset of fission on the pre-scission particle emission probability in the framework of the statistical model. According to Ref. 23, the variation of the fission width Γ_f with time was assumed to be the form

$$\Gamma_f(t) = \Gamma_f(\infty)[1 - \exp(-t/\tau_d)] , \qquad (A1)$$

where $\Gamma_f(\infty)$ was taken to be transition state value of Γ_f

which was calculated by the PACE code. The delay time is defined as τ_d.

The calculation procedure is the same as that of Ref. 23. Since the neutron lifetime $\hbar/\Gamma_n$ is much less than those of proton and ^{4}He, the fission width $\Gamma_f(t)$ was averaged over the neutron lifetime calculated at a given excitation energy and angular momentum of the compound nucleus. Instead of $\Gamma_f(\infty)$, the averaged value of the fission width was used to determine the competition of the particle evaporations and fission. In the successive steps (n) of the particle evapoartion process, the following averaged fission width was used:

$$\int_0^\infty \Gamma_f \left[\sum_{i=1}^{n-1} t_i + t \right] e^{-t/t_n} dt \Big/ \int_0^\infty e^{-t/t_n} dt , \qquad (A2)$$

where t_i is the neutron lifetime in an i step and Γ_f is calculated using the excitation energy after $(n-1)$ neutrons are emitted from the compound nucleus.

The effect of the delayed onset of fission on M_α(CE) becomes remarkable at the high excitation energy region as shown in Fig. 10, because the neutron lifetime becomes shorter than τ_d and then the averaged value of Γ_f becomes smaller than $\Gamma_f(\infty)$.

[1]K. T. R. Davies, A. J. Sierk, and J. R. Nix, Phys. Rev. C **13**, 2385 (1976).

[2]P. Grangé, Li Jun-Qing, and H. A. Weidenmüller, Phys. Rev. C **27**, 2063 (1983).

[3]W. Westmeier and R. A. Esterlund, Z. Phys. A **316**, 27 (1984).

[4]H. Delagrange, C. Grégoire, F. Scheuter, and Y. Abe, Z. Phys. A **323**, 437 (1986).

[5]E. G. Lanza and H. A. Weidenmüller, Z. Phys. A **323**, 157 (1986).

[6]H. A. Weidenmüller, Nucl. Phys. **A471**, 1c (1987).

[7]D. Logan, M. Rajagopalan, M. S. Zisman, J. M. Alexander, M. Kaplan, and L. Kowalski, Phys. Rev. C **22**, 104 (1980).

[8]D. Logan, H. Delagrange, M. F. Rivet, M. Rajagopalan, J. M. Alexander, M. Kaplan, M. S. Zisman, and E. Duek, Phys. Rev. **22**, 1080 (1980).

[9]M. F. Rivet, B. Gatty, H. Guillemot, B. Borderie, R. Bimbot, I. Forest, J. Galin, D. Gardes, D. Guerreau, M. Lefort, X. Tarrago, B. Tamain, and L. Novicki, Z. Phys. A **307**, 365 (1982).

[10]J. M. Alexander, H. Delagrange, M. Rajagopalan, M. F. Rivet, and L. C. Vaz, Z. Phys. A **307**, 149 (1982).

[11]M. Rajagopalan, D. Logan, J. W. Ball, M. Kaplan, H. Delagrange, M. F. Rivet, J. M. Alexander, L. C. Vaz, and M. S. Zisman, Phys. Rev. C **25**, 2417 (1982).

[12]M. F. Rivet, D. Logan, J. M. Alexander, D. Guerreau, E. Duek, M. S. Zisman, and M. Kaplan, Phys. Rev. C **25**, 2430 (1982).

[13]E. Duek, N. N. Ajitanand, J. M. Alexander, D. Logan, M. Kildir, L. Kowalski, L. C. Vaz, D. Guerreau, M. S. Zisman, M. Kaplan, and D. J. Moses, Z. Phys. A **317**, 83 (1984).

[14]L. C. Vaz, D. Logan, E. Duek, J. M. Alexander, M. F. Rivet, M. S. Zisman, M. Kaplan, and J. W. Ball, Z. Phys. A **315**, 169 (1984).

[15]L. Schad, H. Ho, G.-Y. Fan, B. Lindl, A. Pfoh, R. Wolski, and J. P. Wurm, Z. Phys. A **318**, 179 (1984).

[16]N. N. Ajitanand, J. M. Alexander, H. Delagrange, E. Duek,

D. O. Eriksen, D. Guerreau, M. Kaplan, M. Kildir, L. Kowalski, R. Lacey, D. Logan, D. J. Moses, G. F. Peasla, L. C. Vaz, and M. S. Zisman, Z. Phys. A **316**, 169 (1984).

[17]M. Kildir, D. Logan, D. O. Eriksen, D. J. Moses, M. Kaplan, E. Duek, L. C. Vaz, N. N. Ajitanand, J. M. Alexander, and M. S. Zisman, Z. Phys. A **317**, 291 (1984).

[18]D. J. Moses, M. Kaplan, M. Kildir, D. R. G. Logan, G. La Rana, W. E. Parker, R. Lacey, G. F. Peaslee, J. M. Alexander, N. N. Ajitanand, L. C. Vaz, and M. S. Zisman, Nucl. Phys. **A465**, 339 (1987).

[19]Roy Lacey, N. N. Ajitanand, J. M. Alexander, D. M. de Castro Rizzo, G. F. Peaslee, L. C. Vaz, M. Kaplan, M. Kildir, G. La Rana, D. J. Moses, W. E. Parker, D. Logan, M. S. Zisman, P. DeYoung, and L. Kowalski, Phys. Rev. C **37**, 2540 (1988).

[20]E. Holub, D. Hilscher, G. Ingold, U. Jahnke, H. Orf, and H. Rossner, Phys. Rev. C **28**, 252 (1983).

[21]A. Gavron, A. Gayer, J. Boissevain, H. C. Britt, J. R. Nix, A. J. Sierk, P. Grangé, S. Hassani, H. A. Weidenmüller, J. R. Beene, B. Cheynis, D. Drain, R. L. Ferguson, F. E. Obenshain, F. Plasil, G. R. Young, G. A. Petitt, and C. Butler, Phys. Lett. B **176**, 312 (1986).

[22]W. P. Zank, D. Hilscher, G. Ingold, U. Jahnke, M. Lehmann, and H. Rossner, Phys. Rev. C **33**, 519 (1986).

[23]D. J. Hinde, R. J. Charity, G. S. Foote, J. R. Leigh, J. O. Newton, S. Ogaza, and A. Chattejee, Nucl. Phys. **A454**, 550 (1986).

[24]J. O. Newton, D. J. Hinde, R. J. Charity, J. R. Leigh, J. J. M. Bokhorst, A. Chatterjee, G. S. Foote, and S. Ogaza, Nucl. Phys. **A483**, 126 (1988).

[25]D. J. Hinde, H. Ogaza, M. Tanaka, J. Shimoda, N. Takahashi, A. Shinohara, S. Wakamatsu, K. Katori, and H. Okamura, Phys. Rev. C **39**, 2268 (1989).

[26]A. Gavron, Phys. Rev. C **21**, 230 (1980).

[27]J. R. Huizenga and G. Igo, Nucl. Phys. **29**, 462 (1962).

[28]J. M. Alexander, D. Guerreau, and L. C. Vaz, Z. Phys. A **305**,

313 (1982).

[29]R. Lacey, N. N. Ajitanand, J. M. Alexander, D. M. de Castro Rizzo, G. F. Peaslee, L. C. Vaz, M. Kaplan, M. Kildir, G. La Rana, D. J. Moses, W. E. Parker, D. Logan, M. S. Zisman, P. De Young, and L. Kowalski, Phys. Rev. C **37**, 2561 (1988).

[30]G. La Rana, D. J. Moses, W. E. Parker, M. Kaplan, D. Logan, R. Lacey, J. M. Alexander, and R. J. Welberry, Phys. Rev. C **35**, 373 (1987).

[31]F. G. Perey, Phys. Rev. **131**, 745 (1963).

[32]H. Ikezoe, N. Shikazono, Y. Tomita, Y. Sugiyama, K. Ideno, W. Yokota, Y. Nagame, S. M. Lee, M. Ogihara, S. C. Jeong, H. Fujiwara, and D. J. Hinde, Z. Phys. A **330**, 289 (1988).

[33]V. E. Viola, K. Kwiatkowski, and M. Walker, Phys. Rev. C **31**, 1550 (1985).

[34]R. Bass, Nucl. Phys. **A231**, 45 (1974).

[35]M. G. Mustafa, P. A. Baisden, and H. Chandra, Phys. Rev. C **25**, 2524 (1982); A. J. Sierk, Los Alamos National Laboratory Report No. LANL T9.

[36]P. Heeg, K. F. Hoffmann, M. Mutterer, J. P. Theobald, K. Weingärtner, J. Pannicke, F. Gönnenwein, G. Barreau, and B. Leroux, Nucl. Phys. **A409**, 379c (1983).

[37]M. Sowinski, M. Lewitowicz, R. Kupczak, A. Jankowski, N. K. Skobelev, and S. Chojnacki, Z. Phys. A **324**, 87 (1986).

[38]G. L. Catchen, M. Kaplan, J. M. Alexander, and M. F. Rivet, Phys. Rev. C **21**, 940 (1980).

[39]N. N. Ajitanand, G. La Rana, R. Lacey, D. J. Moses, L. C. Vaz, G. F. Peaslee, D. M. de Castro Rizzo, M. Kaplan, and J. M. Alexander, Phys. Rev. C **34**, 877 (1986).

[40]D. J. Moses, M. Kaplan, J. M. Alexander, D. Logan, M. Kildir, L. C. Vaz, N. N. Ajitanand, E. Duek, and M. S. Zisman, Z. Phys. A **320**, 229 (1985).

[41]J. R. Huizanga, A. N. Behkami, I. M. Govil, W. U. Schröder, and J. Tôke, Phys. Rev. C **40**, 668 (1989).

[42]G. F. Peaslee, N. N. Ajitanand, J. M. Alexander, D. Guerreau, R. Lacey, L. C. Vaz, M. Kaplan, M. Kildir, D. J. Moses, D. Logan, and M. S. Zisman, Phys. Rev. C **38**, 1730 (1988).

[43]D. J. Hinde, D. Hilscher, and H. Rossner, Nucl. Phys. **A502**, 479c (1989).

[44]W. D. Myers and W. S. Swiatecki, Ark. Fysik. **36**, 593 (1967).

[45]R. Vandenbosh, T. Murakami, C.-C. Sahn, D. D. Leach, A. Ray, and M. J. Marphy, Phys. Rev. Lett. **56**, 1234 (1986).

[46]O. Tanimura and T. Fliessbach, Z. Phys. A **328**, 475 (1987).

[47]R. Vandenbosch and J. R. Huizenga, *Nuclear Fission* (Academic, New York, 1973).

[48]V. A. Rubchenya and S. G. Yavshits, Z. Phys. A **329**, 217 (1988).

[49]B. Lindl, A. Brucker, M. Bantel, H. Ho, R. Muffler, L. Schad, M. G. Trauth, and J. P. Wurm, Z. Phys. A **328**, 85 (1987).

[50]J. P. Theobald, P. Heeg, and M. Mutterer, Nucl. Phys. **A502**, 343c (1989).